THE COMPANY OF **Biologists**

RESEARCH ARTICLE

Endosomal sorting of VAMP3 is regulated by PI4K2A

Marko Jović[1,‡], Michelle J. Kean[2,3,*], Anna Dubankova[4], Evzen Boura[4], Anne-Claude Gingras[2,3], Julie A. Brill[3,5] and Tamas Balla[1]

ABSTRACT

Specificity of membrane fusion in vesicular trafficking is dependent on proper subcellular distribution of soluble N-ethylmaleimide-sensitive factor attachment protein receptors (SNAREs). Although SNARE complexes are fairly promiscuous *in vitro*, substantial specificity is achieved in cells owing to the spatial segregation and shielding of SNARE motifs prior to association with cognate Q-SNAREs. In this study, we identified phosphatidylinositol 4-kinase IIα (PI4K2A) as a binding partner of vesicle-associated membrane protein 3 (VAMP3), a small R-SNARE involved in recycling and retrograde transport, and found that the two proteins co-reside on tubulo-vesicular endosomes. PI4K2A knockdown inhibited VAMP3 trafficking to perinuclear membranes and impaired the rate of VAMP3-mediated recycling of the transferrin receptor. Moreover, depletion of PI4K2A significantly decreased association of VAMP3 with its cognate Q-SNARE Vti1a. Although binding of VAMP3 to PI4K2A did not require kinase activity, acute depletion of phosphatidylinositol 4-phosphate (PtdIns4P) on endosomes significantly delayed VAMP3 trafficking. Modulation of SNARE function by phospholipids had previously been proposed based on *in vitro* studies, and our study provides mechanistic evidence in support of these claims by identifying PI4K2A and PtdIns4P as regulators of an R-SNARE in intact cells.

KEY WORDS: PI4K2A, VAMP3, PtdIns4P, Vesicle fusion, Sorting, SNARE

INTRODUCTION

Endocytic transport depends on membrane-specific fusion between cargo-containing vesicles and membranes at target compartments. Fusion is mediated by soluble N-ethylmaleimide-sensitive factor (NSF) attachment protein receptor (SNARE) proteins, which form four-helix bundles between a single R-SNARE molecule on the donor vesicle membrane and three cognate Q-SNAREs on the target membrane [Q-SNAREs are SNARES that contribute a glutamine (Q) residue in the formation of the central ionic layer in the assembled core SNARE complex, whereas R-SNAREs contribute

an arginine (R) residue] (Poirier et al., 1998; Sutton et al., 1998). After membrane fusion is complete, the resulting cis-SNARE complex on the target membrane is dissociated by the NSF ATPase and α-soluble NSF attachment protein (α-SNAP) (Mayer et al., 1996; Söllner et al., 1993). Interestingly, although most SNAREs are highly promiscuous *in vitro*, they exhibit a remarkable level of binding preference towards their cognate SNAREs *in vivo* (Brandhorst et al., 2006). Specificity of this interaction is crucial for trafficking of cargoes between different cellular compartments and is achieved through spatial segregation of SNAREs to distinct compartments and even membrane subdomains within individual compartments (McNew et al., 2000; Parlati et al., 2002). Efficiency of SNARE fusion *in vitro* is dependent on the lipid composition of target and donor membranes (Vicogne et al., 2006; Xu and Wickner, 2010). However, how spatial segregation and membrane lipid composition coordinately regulate SNARE-mediated fusion in intact cells remains elusive (Bethani et al., 2007).

Trafficking of SNARE molecules to the correct membranes, as well as shielding of their SNARE motifs from non-physiological SNARE interactions during their transport, are key determinants in sustaining the high level of pairing specificity that R-SNAREs exert towards their cognate Q-SNARE partners (Fasshauer et al., 1998). Maintaining the subcellular localization of SNAREs against a flow of fusion events requires retrieval of R-SNAREs from target membranes and their recycling to correct vesicular donor membranes for successive rounds of fusion. Sorting of SNAREs has been demonstrated to occur independently of cargo sorting, through non-competitive binding to clathrin adaptors (Miller et al., 2011). In addition, proper SNARE pairing might be facilitated by lateral segregation of R-SNAREs to unique membrane subdomains within an individual donor compartment. This is especially important at the sorting endosome, where cargoes directed towards recycling, retrograde or degradative pathways segregate to distinct subdomains of the common compartment (Hsu et al., 2012; Maxfield and McGraw, 2004). VAMP7 and VAMP3 are among key R-SNAREs that co-reside at this compartment, and whereas VAMP7 directly binds adaptor protein complex 3 (AP-3) and regulates fusion with late endosomes, VAMP3 preferentially segregates into tubular membranes, where it facilitates fusion with the endocytic recycling compartment (ERC) and Golgi (McMahon et al., 1993). VAMP3 is a tetanus neurotoxin (TeNT)-sensitive SNARE (Galli et al., 1994; McMahon et al., 1993) that regulates recycling of integrins, transferrin and the transferrin receptor (TfR) to the plasma membrane (Galli et al., 1994; McMahon et al., 1993), as well as α-granule transport in platelets (Feng et al., 2002; Polgár et al., 2002) and retrograde transport of mannose-6 phosphate receptor (M6PR) to the Golgi (Ganley et al., 2008).

PI4K2A is one of the phosphoinositide kinases present at the sorting endosome. As a member of the phosphatidylinositol (PtdIns) 4-kinase family, PI4K2A catalyzes synthesis of PtdIns4P

[1]Section on Molecular Signal Transduction, Program for Developmental Neuroscience, NICHD, NIH, Bethesda, MD 20892, USA. [2]Samuel Lunenfeld Research Institute, 600 University Avenue, Toronto, ON, M5G 1X5, Canada. [3]Department of Molecular Genetics, University of Toronto, 1 King's College Circle, Toronto, ON, M5S 1A8, Canada. [4]Institute of Organic Chemistry and Biochemistry AS CR, v.v.i., Flemingovo nam. 2., 166 10 Prague 6, Czech Republic. [5]Program in Cell Biology, The Hospital for Sick Children, PGCRL, 686 Bay Street, Toronto, ON, M5G 0A4, Canada.
*Present Address: Laboratory of Plant Molecular Biology, The Rockefeller University, 1230 York Avenue, New York, NY 10065, USA.

‡Author for correspondence (jovicm@mail.nih.gov)

in the cell, along with its sister enzyme, PI4K2B, and two type III PI4K enzymes, PI4KA and PI4KB (Balla and Balla, 2006). Among these enzymes, PI4K2A exhibits the most diverse distribution, being present at the Golgi, the trans-Golgi network (TGN) and various endosomal compartments, including sorting, late and recycling endosomes (Craige et al., 2008; Wang et al., 2003). Although the tight membrane association of PI4K2A, mediated through its palmitoyl moieties, implies that this enzyme cycles between endosomes and Golgi (Barylko et al., 2001), it is not known whether and how PI4K2A cycles between these compartments. The importance of PI4K2A endosomal localization is underscored by its role in epidermal growth factor (EGF) receptor degradation (Minogue et al., 2006) and Wnt signaling (Pan et al., 2008). In addition, deletion of the enzyme causes late-onset neurodegeneration (Simons et al., 2009). As a component of the AP-3–BLOC-1 tripartite complex, PI4K2A colocalizes with VAMP7 on sorting endosomes and regulates sorting of lysosome-bound cargoes to late endosomes (Craige et al., 2008; Ryder et al., 2013; Salazar et al., 2009). PI4K2A depletion also results in aberrant localization of the late-endosomal Q-SNAREs Vti1b and syntaxin 8 (Craige et al., 2008). In addition, PI4K2A has been implicated in endocytic recycling, being present on endosomes traversed by endocytosed TfR and angiotensin AT_{1a} receptor en route to the plasma membrane (Balla et al., 2002). Consequently, PI4K2A knockdown results in mislocalization of TfR (Balla et al., 2002; Craige et al., 2008).

In this study, we describe a new interaction between PI4K2A and VAMP3 that is important in sorting and localization of both PI4K2A and VAMP3. We show that targeting of VAMP3 into correct vesicular membranes, where it can mediate fusion with target compartments, requires association with PI4K2A, as well as production of PtdIns4P on endosomal membranes traversed by VAMP3.

RESULTS
An endosomal pool of PI4K2A interacts with VAMP3
PI4K2A localizes to the Golgi and to a diverse pool of endocytic structures, ranging from the early endosome antigen 1 (EEA1)-positive early endosomes to TfR-containing perinuclear recycling endosomes and late endosomes (Balla et al., 2002; Craige et al., 2008; Jović et al., 2012; Salazar et al., 2009; Wang et al., 2003). So far, the best-characterized function of the endosomal pool of PI4K2A is along the lysosomal trafficking route, where it coordinates sorting of lysosomal-associated membrane protein 1 (LAMP-1) and lysosomal integral membrane protein 2 (LIMP-2, also known as SCARB2) (Craige et al., 2008; Jović et al., 2012; Salazar et al., 2009). To further our understanding of the role of PI4K2A in other endosomal compartments, including recycling and retrograde routes, we set out to identify new binding partners using affinity purification coupled to mass spectrometry (AP-MS). Using a FLAG-tagged human PI4K2A stably expressed in HEK293 cells, we analyzed the co-immunoprecipitated binding partners after proteolytic digestion and identification using gel-free mass spectrometry. Among the identified proteins was the SNARE VAMP3 (Fig. 1A; supplementary material Table S1, Fig. S1). Similar to PI4K2A, VAMP3 also localizes to sorting/recycling endosomes (Galli et al., 1994; McMahon et al., 1993), although it has not been linked to regulation of PI4K2A trafficking or function.

Interaction of VAMP3 with PI4K2A was assessed in cells expressing either hemagglutinin (HA)-tagged wild-type PI4K2A

or a HA-tagged catalytically inactive 'kinase-dead' version of the enzyme together with a GFP-tagged VAMP3. Immunoprecipitation of VAMP3 pulled down similar amounts of both enzyme variants, suggesting that this protein–protein interaction does not require the catalytic activity of PI4K2A (Fig. 1B).

VAMP3 regulates the subcellular distribution of PI4K2A
Given that both VAMP3 and PI4K2A are known to localize to TfR-containing endosomes (Balla et al., 2002; Galli et al., 1994; McMahon et al., 1993), we compared their distribution by live-cell imaging in COS-7 cells co-expressing low levels of GFP–VAMP3 and monomeric red fluorescent protein (mRFP)-tagged PI4K2A. VAMP3 showed colocalization with PI4K2A on endosomal structures, as well as peripheral tubules, which was corroborated by the endogenous staining (Fig. 1C,D). Given the role of VAMP3 in recycling and retrograde trafficking, we assessed the functional relevance of its interaction with PI4K2A by blocking VAMP3-mediated fusion using TeNT light chain overexpression. TeNT specifically cleaves VAMP3 in non-neuronal cells (Galli et al., 1994), and we determined its efficacy by co-expressing the N-terminally tagged GFP–VAMP3 together with TeNT light chain, so that cleavage would be expected to result in appearance of the GFP-tagged VAMP3 N-terminus in the cytosol. We found that Golgi localization of endogenous PI4K2A markedly decreased in TeNT-expressing cells (Fig. 2A). This effect was successfully prevented by co-transfection of a TeNT-resistant VAMP3, GFP–VAMP3 VW (Regazzi et al., 1996) together with TeNT light chain (Fig. 2B), indicating that VAMP3 participates in retrograde transport of PI4K2A from the endosomal pool back to the Golgi.

Next, we measured the role of VAMP3 in controlling the rate of PI4K2A retrograde transport in live COS-7 cells. For this, we used fluorescence recovery after photobleaching (FRAP) of GFP–PI4K2A. Following photobleaching of the pericentriolar area containing the Golgi, recovery of PI4K2A fluorescence was largely driven by the rate of its retrograde transport (Fig. 2C). Expression of TeNT substantially delayed this process, indicating that VAMP3-mediated fusion contributes to retrograde trafficking of PI4K2A (Fig. 2C,D).

Proper VAMP3 targeting requires PI4K2A
Although VAMP3 regulates trafficking of various other proteins, including PI4K2A (see above), little is known about the sorting of VAMP3 itself to the cellular compartments where it facilitates fusion. Given the interaction between PI4K2A and VAMP3, we used RNA interference (RNAi)-mediated knockdown of PI4K2A to explore whether the endosomal pool of PI4K2A plays a role in VAMP3 sorting. COS-7 cells were treated with short interfering RNA (siRNA) targeting PI4K2A for 2 days (Fig. 3A), followed by transfection with the VAMP3–HA construct for 1 day. Cells were then fixed and immunostained for PI4K2A and HA. Knockdown of PI4K2A led to accumulation of VAMP3–HA on enlarged endosomes, suggesting a trafficking defect (Fig. 3A, bottom). To measure the potential missorting of VAMP3 in live cells, we next expressed GFP–VAMP3 together with the late-endosomal- and lysosomal-resident protein LAMP-1–mRFP. There was little overlap in the distribution of these two molecules in live COS-7 cells treated with control siRNA (Fig. 3B). However, depletion of PI4K2A resulted in missorting of VAMP3 onto LAMP-1-positive enlarged vesicles (Fig. 3B, bottom). These structures have previously been described as being a hallmark of PI4K2A
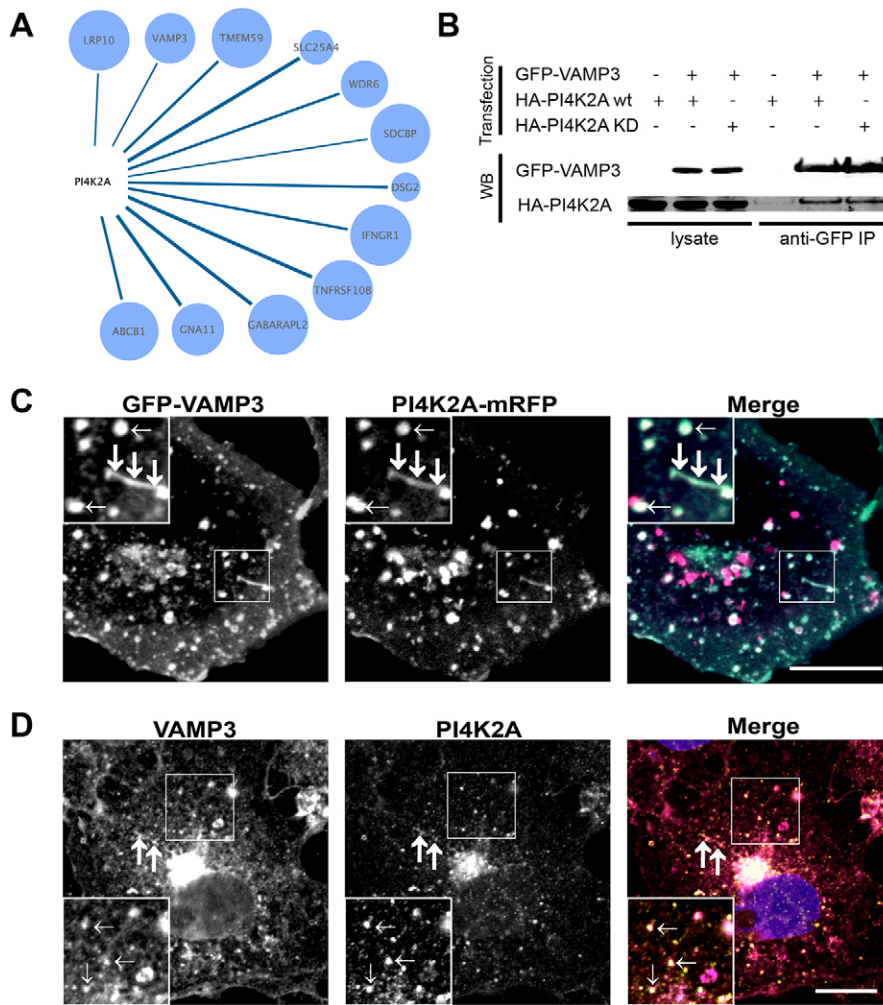
Fig. 1. Identification of VAMP3 binding to PI4K2A. (A) AP-MS analysis of PI4K2A was performed in HEK293 cells stably expressing FLAG–PI4K2A (see Materials and Methods). The sizes of the nodes (blue circles) represent the frequency of the protein identified in our internal database. The thickness of the lines represents the number of unique peptides identified in the analysis (a thicker line represents more peptides identified). See supplementary material Table S1 for details. (B) COS-7 cells co-transfected with GFP–VAMP3 and either HA–PI4K2A wt or kinase dead (KD) were immunoprecipitated (IP) using anti-GFP beads. Total cell lysates and eluted immunoprecipitated samples and were resolved by SDS-PAGE and analyzed by immunoblotting (WB), using anti-GFP (top) or anti-HA antibody (bottom). (C) Live-cell imaging of COS-7 cells expressing GFP–VAMP3 and PI4K2A–mRFP. (D) Endogenous distribution of VAMP3 and PI4K2A. COS-7 cells were fixed, permeabilized and incubated with rabbit polyclonal antibody against VAMP3 and 4C5G mouse monoclonal antibody against PI4K2A. Enlargements of the boxed area are shown in the insets. The thick arrows indicate tubular structures and thin arrows indicate vesicles. Scale bars: 10 μm.

knockdown, best observed in live cells (Craige et al., 2008). VAMP3 was primarily missorted into Rab7-positive late endosomes, without significant overlap with either early or recycling endosomes (Fig. 3D). The degree of overlap between VAMP3 and LAMP-1 was measured using Pearson's correlation coefficient (r), which revealed a substantial increase in correlation between pixel intensities in the two channels upon PI4K2A depletion (Fig. 3C). These findings, therefore, indicate a requirement for PI4K2A in efficient VAMP3 sorting.

VAMP3 reaches its target compartments through a PI4K2A-dependant mechanism

Sufficient levels of VAMP3 are needed to facilitate fusion with target compartments, namely the Golgi, recycling endosomes and the plasma membrane. Given the role of PI4K2A in VAMP3 sorting, a process that precedes fusion with target membranes, we measured VAMP3 at the plasma membrane and the perinuclear Golgi/recycling membranes following PI4K2A knockdown.

The plasma membrane pool of VAMP3 was detected in non-permeabilized cells expressing a VAMP3 construct with an HA tag fused to the extracellular C-terminus, as previously described (Gordon et al., 2009). Cell surface levels of VAMP3–HA were substantially lower in PI4K2A-knockdown cells than in cells treated with control siRNA, as shown by confocal microscopy (Fig. 4A). Flow cytometry analysis of cells with greater than 80% knockdown of PI4K2A showed a significant decrease in surface

VAMP3 levels upon PI4K2A depletion, without an overall change in total VAMP3 (Fig. 4B,C). Similarly, treatment of cells with siRNA targeting the PI4K2A 3′ untranslated region (3′UTR) decreased VAMP3 surface levels, whereas re-expression of PI4K2A fully rescued this phenotype (Fig. 4D).

Interestingly, the appearance of VAMP3 on the plasma membrane is also dependent on the catalytic activity of PI4K2A. Overexpression of the GFP–PI4K2A kinase-dead mutant, but not the wild-type kinase, significantly reduced cell surface levels of VAMP3 (Fig. 4E). Dominant-negative effects of kinase-dead mutants of PI4Ks have previously been documented for the kinase-dead PI4K2B (Balla et al., 2005). Steady-state levels of VAMP3 on target membranes, therefore, are directly dependent on PI4K2A availability, as well as its activity.

To measure the kinetics of VAMP3 appearance on perinuclear membranes in live cells, we performed FRAP time-lapse microscopy. To this aim, cells knocked down for PI4K2A and transfected with GFP–VAMP3 were photobleached at the perinuclear recycling endosome and Golgi. The rate of FRAP at these membranes was found to be substantially reduced in cells treated with PI4K2A siRNA compared to control siRNA (Fig. 4F,G). In contrast, inhibition of the Golgi-localized type III PI4K, PI4KB, using PIK93, a potent inhibitor of this enzyme ($IC_{50}=19$ nM) (Balla et al., 2008; Knight et al., 2006), did not affect the rate of fluorescence recovery of VAMP3 signal in these compartments (Fig. 4G).
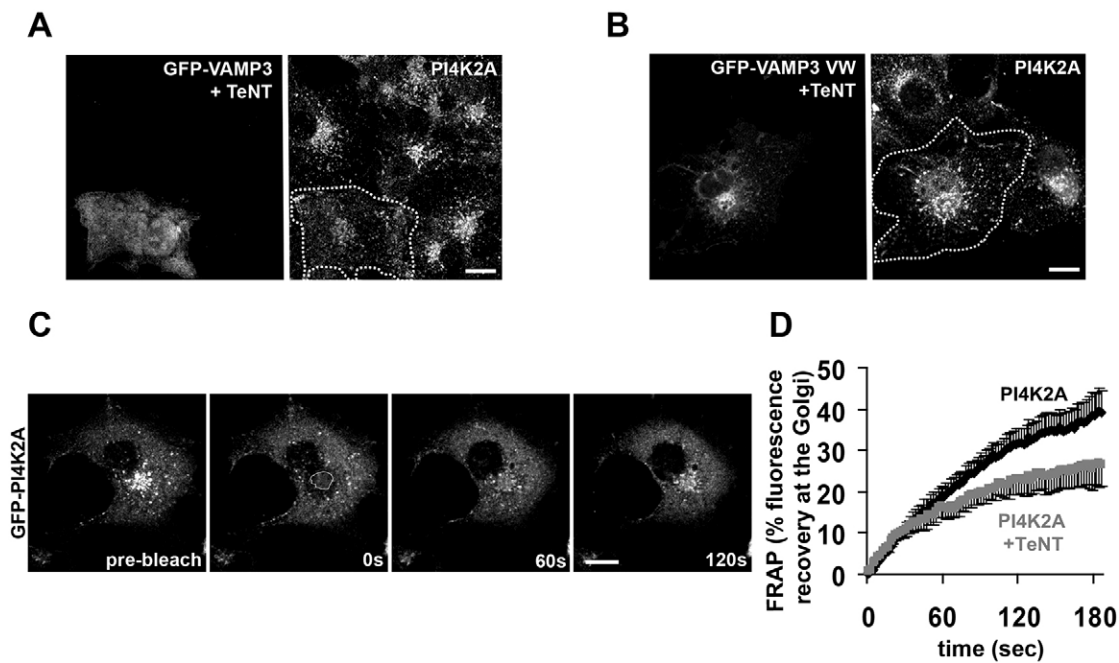
Fig. 2. PI4K2A localization is affected by VAMP3 inactivation. (A,B) Fluorescence micrographs of COS-7 cells co-transfected with TeNT and either GFP–VAMP3 wt (A) or the GFP–VAMP3 VW mutant (B). Fixed cells were stained with a rabbit polyclonal antibody against PI4K2A (right panels). The dotted line indicates the cell outline. (C,D) Retrograde transport of PI4K2A following photobleaching of the perinuclear and Golgi compartment in COS-7 cells expressing GFP–PI4K2A. (C) Sequential imaging during photobleaching. (D) The rate of FRAP was faster in cells transfected with GFP–PI4K2A alone (black, $n=10$), than in those coexpressing GFP–PI4K2A and TeNT (gray, $n=10$). Shown are mean fluorescence intensity curves +s.e.m. (PI4K2A alone) or –s.e.m. (PI4K2A + TeNT), plotted as described in the Materials and Methods. Scale bars: 10 μm.

PI4K2A is necessary for the formation of SNARE complexes

If PI4K2A affects the availability of VAMP3 at the target membrane, then it is also expected that PI4K2A depletion would decrease VAMP3 pairing with Q-SNAREs. One of the documented VAMP3 cognate Q-SNAREs on perinuclear Golgi membranes is Vti1a (Mallard et al., 2002). Together with syntaxin 10 and syntaxin 16, Vti1a participates in a VAMP3 fusion complex that facilitates retrograde transport of M6PR and Shiga toxin back to the Golgi (Ganley et al., 2008; Mallard et al., 2002). Given the effects of PI4K2A depletion on VAMP3 localization, we looked into the potential impact of PI4K2A knockdown on the distribution of Vti1a. Cells with efficient PI4K2A knockdown did not show a notable redistribution of Vti1a (Fig. 5A). To further test whether PI4K2A plays a role in interactions of VAMP3 with its cognate SNAREs, we took advantage of the inhibitory effect of N-ethylmaleimide (NEM) on SNARE complex disassembly. As previously described, treatment of cells with NEM blocks disassembly of cis-SNARE complexes, including Vti1a–VAMP3 complexes, on target membranes (Mallard et al., 2002). NEM, therefore, effectively 'captures' VAMP3 on the target membranes, preventing the subsequent recycling to vesicular membranes (Fig. 5B). Although little Vti1a was co-immunoprecipitated in complex with VAMP3, NEM treatment significantly increased the number of Vti1a molecules detected in the cis complex (Fig. 5C–E). This increase in Vti1a binding was greatly reduced with prior PI4K2A siRNA treatment. These findings are consistent with our conclusion that PI4K2A primarily exerts its role in VAMP3 sorting at an endosomal compartment, thereby preventing VAMP3 from reaching its cognate SNAREs.

Efficient VAMP3 sorting requires endosomal PtdIns4P

Although kinase activity does not affect PI4K2A binding to VAMP3 (Fig. 1B), this result does not exclude the potential role of a localized supply of PtdIns4P lipid on endosomal membranes in the subsequent sorting of VAMP3. To test this possibility, we acutely depleted PtdIns4P on VAMP3 endosomes. This was achieved by rapamycin-induced recruitment of a cytosolic variant of the PtdIns4P phosphatase Sac1 (lacking the ER-localization sequence) to VAMP3-positive endosomes. We used the type I integral TGN protein, Tgn38, fused to the FKBP12-rapamycin-binding (FRB) domain of mammalian target of rapamycin (mTOR) as a recruiter molecule. Tgn38 cycles between the TGN and plasma membrane in VAMP3-containing endosomes, where VAMP3 facilitates delivery of Tgn38 to target compartments. Under such an experimental setup, rapamycin addition induces rapid heterodimerization of the FRB domain with the FKBP12 module fused to cytosolic Sac1, resulting in recruitment of Sac1 and acute dephosphorylation of PtdIns4P at Tgn38-containing membranes (Szentpetery et al., 2010).

Effects of PtdIns4P elimination were studied in cells transfected with cyan fluorescent protein (CFP)-tagged Tgn38–FRB (Tgn38–FRB–CFP), together with GFP–VAMP3 and monomeric red fluorescent protein (mRFP)-tagged FKBP12–Sac1 (mRFP–FKBP12–Sac1). VAMP3 was found to co-reside with Tgn38 on peripheral endocytic vesicles, in addition to the late Golgi compartment and recycling endosomes that together form the perinuclear VAMP3 compartment (Fig. 6A; supplementary material Fig. S2). Addition of rapamycin resulted in rapid redistribution of the cytosolic Sac1 phosphatase to Tgn38 membranes (Fig. 6B,C). At 15 min following recruitment of mRFP–FKBP12–Sac1 (or mRFP–FKBP12 as a control), we
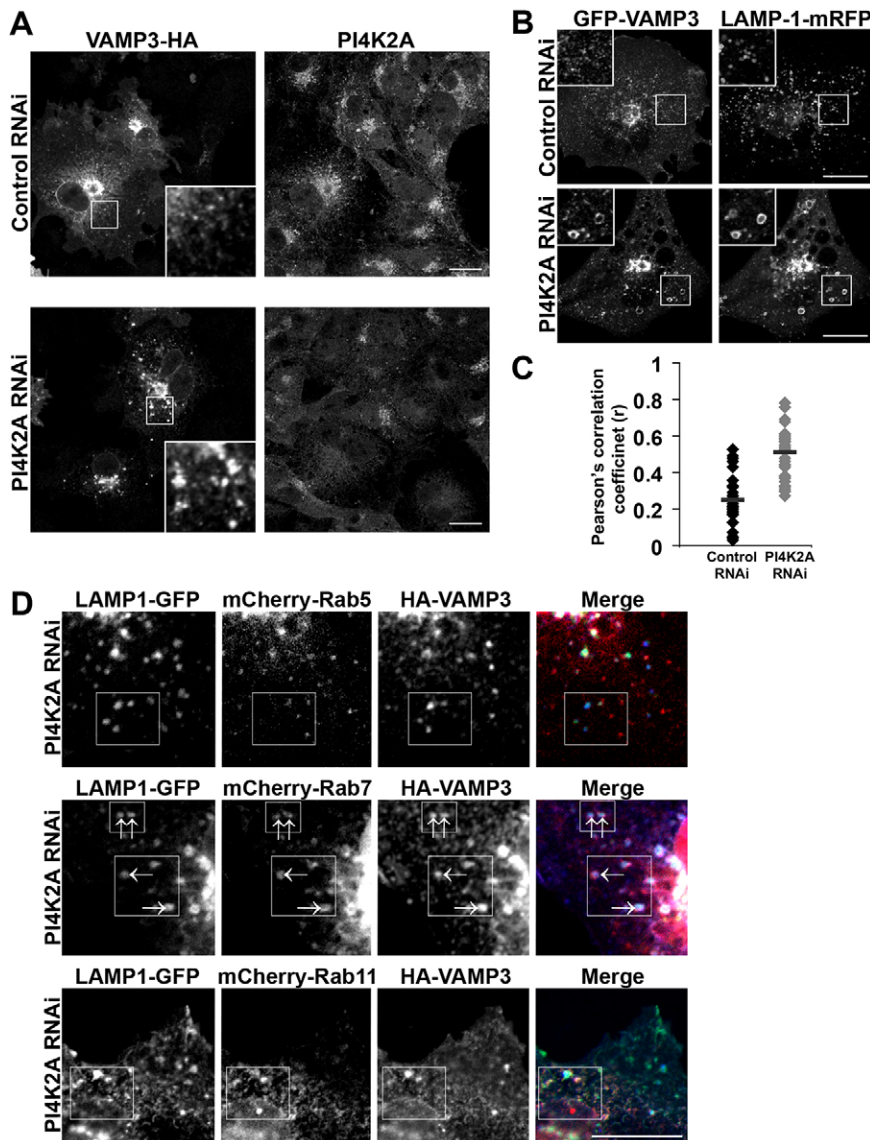
Fig. 3. PI4K2A regulates VAMP3 sorting. (A) COS-7 cells were treated with control siRNA or siRNA directed against PI4K2A for 2 days prior to transfection with VAMP3–HA. At 1 day after transfection, cells were fixed, permeabilized and incubated with rabbit polyclonal antibody against PI4K2A and mouse monoclonal antibody against the HA epitope. PI4K2A knockdown resulted in an accumulation of VAMP3 on enlarged vesicles. (B–D) Live-cell confocal microscopy of COS-7 cells after a 2-day treatment with control or PI4K2A siRNA duplexes and co-transfection with GFP–VAMP3 and either LAMP-1–mRFP (B,C) or mCherry–Rab5, mCherry–Rab7 or mCherry–Rab11 (D). (C) Comparison of GFP–VAMP3 and LAMP-1–mRFP pixel (Pearson's) correlation coefficients. (D) PI4K2A depletion results in missorting of VAMP3 into enlarged LAMP1- and Rab7-containing compartments (control siRNA, $n=27$; PI4K2A siRNA, $n=31$). Enlargements of the boxed area are shown in the insets for A and B. The boxes in D represent VAMP3-enriched vesicles; arrows indicate Rab colocalization. Scale bars: 10 µm.

photobleached the perinuclear pool of GFP–VAMP3 colocalizing with Tgn38. Recruitment of mRFP–FKBP12 alone did not affect the rate of VAMP3 reappearance in these compartments, whereas mRFP–FKBP12–Sac1 recruitment dramatically delayed this process (Fig. 6D).

Given that the recruitment mediated by Tgn38 spans several VAMP3-containing compartments, we further dissected the individual contributions of the Golgi, plasma membrane and endosomal pools of PtdIns4P using compartment-specific recruiters (Fig. 6E). PtdIns4P depletion at the plasma membrane, using the plasma membrane localization sequence of Lyn kinase (PM2–FRB–CFP) (Inoue et al., 2005), did not significantly affect the rate of VAMP3 trafficking. Recruitment of Sac1 exclusively to the Golgi, using FRB–CFP–Giantin (Komatsu et al., 2010), did cause a delay in VAMP3 delivery to the perinuclear compartment. However, recruitment by Tgn38 to endosomal membranes, in addition to the Golgi compartment, resulted in a larger delay in the rate of VAMP3 transport. Availability of PtdIns4P on VAMP3 endosomes is, therefore, a crucial factor in subcellular movement of this R-SNARE.

PI4K2A and VAMP3 regulate endocytic recycling of transferrin

VAMP3 facilitates the membrane fusion that is necessary for efficient transport of endocytosed transferrin (Galli et al., 1994; McMahon et al., 1993), a canonical recycling cargo previously shown to traverse PI4K2A-positive endosomes en route to the ERC (Balla et al., 2002; Craige et al., 2008). Interestingly, PI4K2A knockdown has been found to induce mislocalization of the TfR into an enlarged endosomal compartment (Craige et al., 2008), similar to the VAMP3 mislocalization observed in the present study in PI4K2A-depleted cells (Fig. 3B). To assess the potential role of PI4K2A in transferrin recycling, we first examined its contribution to the delivery of labeled transferrin from the endosomal VAMP3 compartment to the perinuclear ERC, one of the VAMP3 target compartments. After a 30-min serum starvation, a 10-min pulse with fluorophore-conjugated transferrin was performed in cells previously treated with either PI4K2A or control siRNA for 3 days (Fig. 7A). PI4K2A knockdown induced a significant delay in transferrin delivery to the recycling compartment, similar to the effect of TeNT
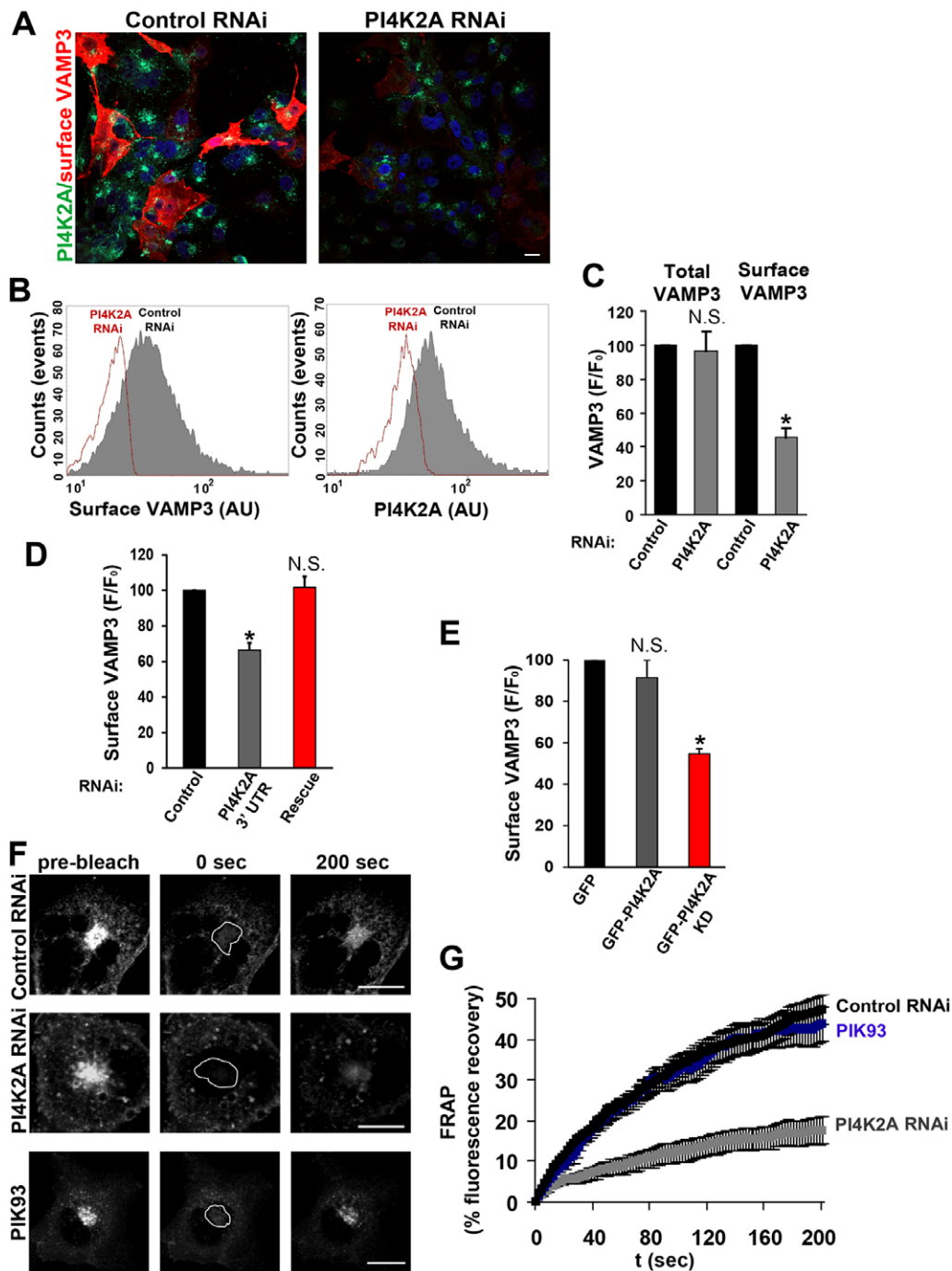
Fig. 4. VAMP3 levels on target membranes depend on PI4K2A. (A–D) VAMP3–HA was expressed in control or PI4K2A siRNA-treated cells, followed by fixation and immunostaining against HA epitope under non-permeabilizing conditions. Cells were then permeabilized, stained with an antibody against PI4K2A (A–D) and DAPI (A), for analysis either by confocal microscopy (A) or flow cytometry (B–D). Cell-surface levels of VAMP3 were reduced in PI4K2A knockdown cells (red) in comparison to control knockdown (gray) (n=10,000 cells). (C) Surface or total levels of VAMP3 in control siRNA-treated cells (black) were compared to gated cells showing >80% PI4K2A knockdown (grey). Results are mean±s.e.m. (n=5; 10,000 cells per sample). *P<0.05 (two-tailed Student's t-test), N.S., not statistically significant (P=0.77). (D) Reduced cell-surface levels of VAMP3 in PI4K2A knockdown cells (gray) were rescued by expression of PI4K2A–GFP (red) to levels that did not show statistical significance in comparison to the control knockdown (black) as determined by one-way ANOVA. *P<0.05; N.S., not statistically significant (n=4; 10,000 cells per sample). (E) VAMP3 surface levels in cells transfected with VAMP3–HA and either GFP only (black), PI4K2A–GFP (gray) or the PI4K2A–GFP kinase dead (KD) mutant (red) were determined by flow cytometry. Overexpression of catalytically dead, but not the wild-type PI4K2A, induced a significant decrease in cell surface levels, based on one-way ANOVA. *P<0.05; N.S., not statistically significant (n=4; 10,000 cells per sample). (F,G) VAMP3 fluorescence recovery was recorded in COS-7 cells transfected with GFP–VAMP3 after 2-day treatment with control siRNA (black, n=27) or siRNA directed against PI4K2A (gray, n=32), or 16 h incubation with 100 nM PIK93, an inhibitor of PI4KB (blue, n=29). The outlined area in F represents the area bleached. Only PI4K2A knockdown induced a substantial delay in fluorescence recovery. FRAP measurements represent mean±s.e.m. for three independent experiments (see Materials and Methods). AU, arbitrary units. Scale bars: 10 µm.
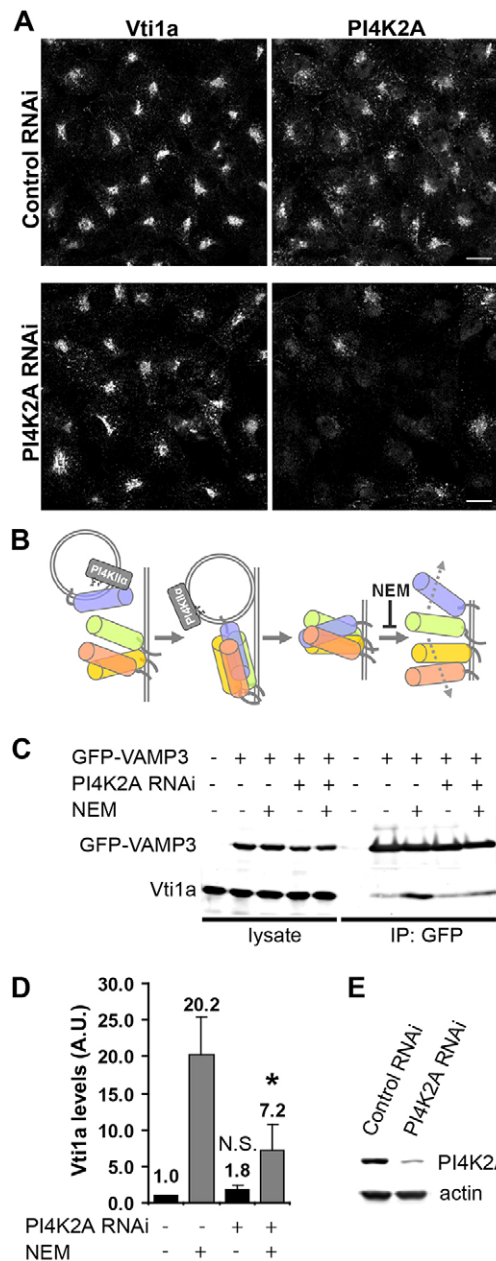
Fig. 5. PI4K2A is required for VAMP3 interaction with cognate Q-SNARE Vti1a. (A) COS-7 cells were transfected with control siRNA or siRNA directed against PI4K2A for 2 days, fixed, then permeabilized and incubated with a rabbit polyclonal antibody directed against PI4K2A and a mouse monoclonal antibody directed against Vti1a. (B) The cartoon depicts the proposed role of PI4K2A (blue) in sorting of VAMP3 (lavender) to endosomal membranes, where it engages in SNARE complex formation with Vti1a (green) and other cognate Q-SNAREs. NEM inhibits disassembly of the complex, trapping Vti1a bound to VAMP3. (C) COS-7 cells were treated for 2 days with control or PI4K2A siRNA, transfected with GFP–VAMP3, and either preincubated with 1 mM NEM for 30 min or directly lysed. GFP–VAMP3 was immunoprecipitated from total cell lysates using anti-GFP beads. Immunoprecipitated samples were eluted and analyzed by SDS–PAGE, followed by western blotting. (D) Quantification of Vti1a present in complex with VAMP3 in immunoprecipitated samples, as shown in C. Results are mean±s.e.m. from five experiments. *$P<0.05$ between NEM-treated samples, as determined by one-way ANOVA analysis; N.S. not significant compared with control. (E) Assessment of PI4K2A knockdown from the experiment shown in C. After 72 h of treatment with control or PI4K2A siRNA, cells were lysed and analyzed by western blotting using antibodies against PI4K2A and actin. A.U., arbitrary units. Scale bars: 10 μm.

overexpression (Fig. 7B). Importantly, PI4K2A depletion did not affect ERC morphology, such that after a prolonged pulse of 20 min we did observe transferrin accumulation in the ERC even in cells with no detectable PI4K2A (supplementary material Fig. S3). Hence, PI4K2A knockdown results in a delay rather than a complete blockage of this process.

To test whether the delay in transferrin trafficking to the ERC had an impact on overall transferrin recycling, we measured total levels of internalized labeled transferrin after a 30-min chase in complete medium. Flow cytometry analysis showed that PI4K2A depletion consistently slowed the overall rate of transferrin recycling (Fig. 7C), resulting in a 45% higher retention of internalized transferrin in cells in which PI4K2A knockdown was greater than 80% (Fig. 7D). Taken together, these findings reveal the importance of PI4K2A and VAMP3 for efficient TfR recycling.

DISCUSSION

In this study, we show that the interaction between PI4K2A and VAMP3 is important both for proper PI4K2A trafficking between the Golgi and endosomal compartments, and for the movement and distribution of the R-SNARE VAMP3. Furthermore, we provide evidence in intact cells that endosomal PtdIns4P is required for delivery of VAMP3 to the proper endosomal compartments, where it can facilitate fusion.

Although PI4K2A activity has been linked to trafficking at various compartments, including the Golgi, late and recycling endosomes, the mechanism regulating overall PI4K2A distribution among these compartments remains poorly understood. Transport of PI4K2A to late endosomes is mediated through the interaction of AP-3 with a dileucine motif in PI4K2A, an interaction that is crucial for sorting of the lysosomal proteins LAMP-1 and LIMP-2 (Craige et al., 2008; Jović et al., 2012). The question still remains as to how PI4K2A is retrieved from endosomal compartments to the Golgi. Here, we demonstrate that retrograde transport of PI4K2A depends on VAMP3, such that cleavage of VAMP3 results in PI4K2A accumulation on endosomal membranes.

Interestingly, our PI4K2A AP-MS identified one peptide of another endosomal R-SNARE, VAMP7, suggesting a potential PI4K2A–VAMP7 interaction (VAMP7 spectra in supplementary material Fig. S4). This finding corroborates the previously documented colocalization of VAMP7 with PI4K2A on late endosomes and association of VAMP7 with AP-3 (Craige et al., 2008; Martinez-Arca et al., 2003). Taken together, these findings suggest that PI4K2A localization is maintained by opposing trafficking forces exerted by AP-3 and associated molecules, like VAMP7, in the direction of lysosomes, and VAMP3-dependent transport towards the Golgi and recycling endosomes. Perturbation of either sorting mechanism, therefore, could result in redistribution of PI4K2A to the opposing arm of the pathway.

Our data also indicate that PI4K2A is not simply a cargo that relies on VAMP3-mediated fusion, but acts as an integral component of the pathway, regulating sorting of VAMP3. R-SNARE sorting has been proposed to modulate SNARE pairing specificity *in vivo* (Bethani et al., 2007). This is particularly evident at the level of the sorting endosome, which is traversed by several different R-SNAREs that engage in fusion at various target organelles (Brandhorst et al., 2006). Homotypic fusion of sorting endosomes is primarily mediated by a single residing R-SNARE, VAMP4, that pairs with the Q-SNAREs syntaxin 13, syntaxin 6 and Vti1a (Brandhorst et al., 2006). This pairing specificity is maintained *in vivo* in spite of the ability of other
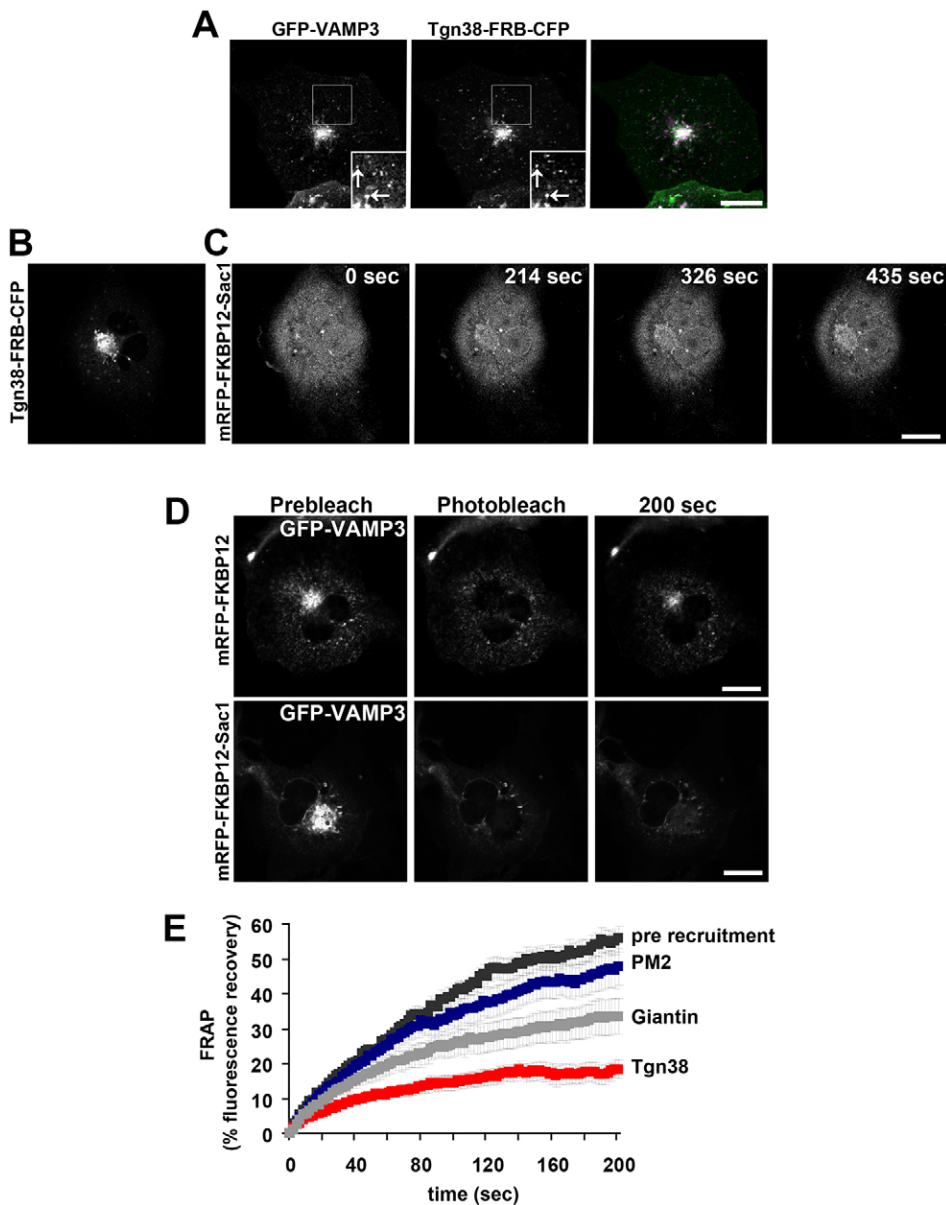
Fig. 6. Acute depletion of endosomal PtdIns4P reduces the rate of VAMP3 appearance at the target membranes. (A) COS-7 cells co-expressing mRFP–FKBP12–Sac1 and Tgn38–FRB–CFP imaged by live-cell confocal microscopy. Enlargements of the boxed area are shown in the insets. The arrows indicate vesicles containing VAMP3 and Tgn38. (B,C) Cells co-expressing Tgn38–FRB–CFP (B) and mRFP–FKBP12-Sac1 (C) were mounted on the heated stage of the microscope (35°C) and treated with 100 nM rapamycin to induce recruitment of the cytosolic Sac1 to the Golgi. Time-lapse images of individual cells were recorded for 10 min. (D) FRAP analysis in cells co-transfected with GFP–VAMP3, Tgn38–FRB–CFP and either mRFP–FKBP12 (upper panels) or mRFP–FKBP12–Sac1 (lower panels). At 10 min after rapamycin addition, the perinuclear and Golgi pool of GFP–VAMP3 was photobleached and fluorescence recovery was imaged by time-lapse microscopy. Representative images of cells with efficient recruitment show delayed GFP–VAMP3 fluorescence recovery after Sac1 recruitment (lower panel), as compared to FKBP12 alone (upper panel). (E) COS-7 cells expressing GFP–VAMP3, mRFP–FKBP12–Sac1 and either Tgn38, Giantin or PM2 tagged with FRB–CFP were treated for 10 min with 100 nM rapamycin, followed by FRAP recording of the GFP signal in the perinuclear and Golgi area. Each value represents mean fluorescence recovery ($\pm$s.e.m.) (pre-recruitment, $n=17$; PM2, $n=18$; Giantin, $n=15$; Tgn38, $n=18$). Scale bars: 10 µm.

R-SNAREs passing through the sorting endosome to bind the VAMP4 cognate SNAREs *in vitro* (Brandhorst et al., 2006; Fasshauer et al., 1999).

Selectivity in SNARE preference *in vivo* has been proposed to occur through spatial segregation of SNAREs to membrane microdomains within a single vesicular compartment, resulting in shielding of the passing SNAREs from non-specific interactions. At the level of sorting endosomes, PtdIns3P has long been recognized as a lipid determinant of such a microdomain (Bethani et al., 2007; Gillooly et al., 2000; Gillooly et al., 2003). At the same time, an increasing body of evidence suggests that PtdIns4P-rich membranes also play important roles in sorting processes at endosomal compartments, independent of PtdIns3P. Recruitment of AP-3 to sorting endosomes and trafficking of cargos to lysosomes, lysosome-related organelles and synaptic vesicles have all been linked to PtdIns4P produced by endosomal PI4K2A (Burgess et al., 2012; Craige et al., 2008; Guo et al., 2003; Jović et al., 2012). Here, we demonstrate that PI4K2A and VAMP3 colocalize on tubulo-vesicular recycling membranes,

and that downregulation of PI4K2A, as well as acute depletion of PtdIns4P from those compartments, significantly perturbs sorting of VAMP3. PI4K2A knockdown led to missorting of VAMP3 to late endosomes and away from recycling membranes, resulting in decreased interaction with the cognate SNARE Vti1a and causing delayed delivery of TfR to the ERC. Given the established role of VAMP3 in endocytic recycling of TfR, these findings also clarify the previously documented, yet poorly understood, role of PI4K2A in this process. It is noteworthy that recycling of other cargoes, such as the angiotensin AT_{1a} receptor and glucose transporter GLUT4, has previously been shown to require PI4K2A and VAMP3 (Balla et al., 2002; Rothenberger et al., 2007; Volchuk et al., 1995; Xu and Wickner, 2010), suggesting a more ubiquitous role for PI4K2A in this pathway.

Although this is the first study to show interaction between a SNARE and a lipid-modifying enzyme involved in SNARE sorting, trafficking of VAMP3 has previously been linked to phosphoinositides. Endocytosis of VAMP3 requires the clathrin assembly lymphoid myeloid (CALM) adaptor protein, which
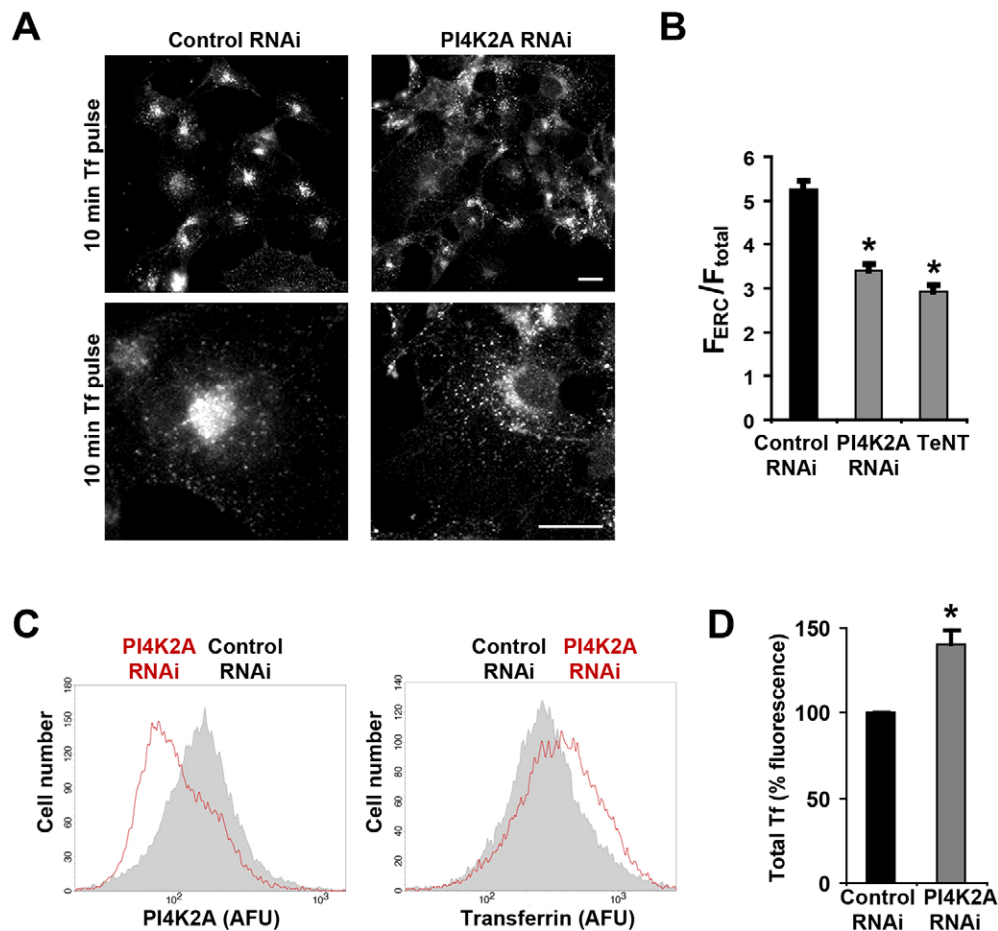
Fig. 7. TfR delivery to the ERC and rate of recycling are reduced upon PI4K2A depletion. After treatment of COS-7 cells with control siRNA or siRNA directed against PI4K2A, cells were serum-starved for 30 min, then incubated with Alexa-Fluor-488-conjugated transferrin for 10 min and either fixed (A,B) or chased in complete medium for 30 min prior to fixation in 4% paraformaldehyde (C,D). PI4K2A knockdown (A, right panel) impedes delivery of transferrin to the ERC in comparison to the control siRNA-treated cells (A, left panels). (B) Appearance of transferrin in the perinuclear ERC in cells treated with siRNA oligonucleotides, shown in A, or transfected with TeNT. The ratio of transferrin fluorescence in the ERC (F_{ERC}) and total fluorescence (F_{total}) was determined as described in the Materials and Methods. Shown are ratios of mean+s.e.m. fluorescence values ($n=50$). Statistical significance was determined by one-way ANOVA analysis. *$P<0.05$ for control versus PI4K2A knockdown and control versus TeNT). (C) Total levels of internalized transferrin, as determined by flow cytometry. Following fixation, cells were incubated with a rabbit polyclonal antibody against PI4K2A. Graphs depict endogenous levels of PI4K2A and total levels of transferrin following a 30 min chase in a representative experiment ($n=3$). (D) Total intracellular levels of internalized transferrin, as described in C, in cells gated for a PI4K2A knockdown efficiency of >80%. Graph represents mean±s.e.m. fluorescence intensity ($n=3$ experiments, 10,000 cells per sample). AFU, arbitrary fluorescence units. Scale bars: 10 μm.

simultaneously interacts with VAMP3 and PtdIns(4,5)P_2 molecules (Miller et al., 2011). Dephosphorylation of PtdIns(4,5)P_2 by 5-phosphatase enzymes during endocytosis results in decreased affinity of CALM towards VAMP3 and causes disassembly of the complex (Miller et al., 2011). Once internalized, VAMP3 passes through PtdIns3P-enriched early endosomes (Naughtin et al., 2010) (Fig. 8), but it is not known whether PtdIns3P has any role in VAMP3 trafficking at this compartment.

What could be the mechanism by which PtdIns4P affects VAMP3 distribution? Previous studies have suggested that negatively charged phospholipids stabilize the SNARE motif prior to fusion (Ellena et al., 2009). During formation of a trans-SNARE fusion complex, the N-termini of an R-SNARE and opposing Q-SNAREs form an initial contact that is followed by a zippering association into a fusion complex. For the initial interaction to occur, the natively disordered SNARE motif of an R-SNARE needs to adopt a helical structure at its N-terminal

helix I, which then serves as a folding nucleus for the rest of the unstructured SNARE motif, allowing subsequent zippering and fusion (Ellena et al., 2009). Interestingly, the initial folding of helix I of the VAMP3 neuronal homolog VAMP2 depends on the presence of lipids. Association of the hydrophobic surface of the initially unstructured N-terminus with micellar lipids has been found to stabilize the transient helix I and to promote further folding of the rest of the SNARE motif *in vitro* (Ellena et al., 2009). Although amphipathic helices lack lipid-binding specificity, the role of PtdIns4P could be functionally relevant, given the high local concentration of PtdIns4P in VAMP3-adjacent membranes as a result of PI4K2A binding (Fig. 8). The specificity, therefore, is a result of VAMP3 interaction with the kinase that produces the lipid for interaction with the VAMP protein.

Taken together, the interaction between VAMP3 and PI4K2A establishes a paradigm for the regulatory role of phosphoinositide kinases in SNARE sorting. Based on our evidence in intact cells
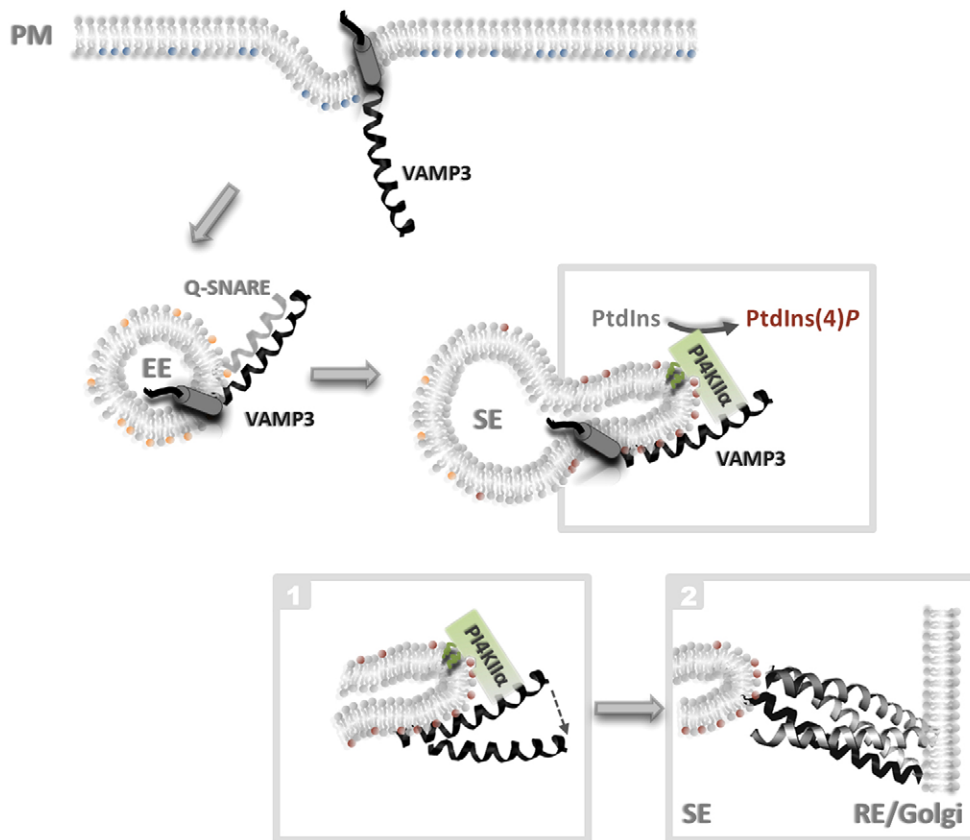
Fig. 8. PI4K2A and PtdIns4P regulate VAMP3 sorting. Following VAMP3 endocytosis at the PtdIns(4,5)P_2-rich plasma membrane subdomains (blue), VAMP3 passes through early endosomal compartments containing PtdIns(3)P (orange), prior to delivery to sorting endosomes enriched with PtdIns(4)P (brown). Availability of PI4K2A for interaction with VAMP3, along with the catalytic activity of PI4K2A, ensures proper sorting of VAMP3 within this compartment, a process that is a prerequisite for efficient interaction of VAMP3 with cognate Q-SNAREs, such as Vti1a, on target membranes.

that PtdIns4P is required for VAMP3 transport, we propose that R-SNARE sorting depends on segregation away from non-physiological binding partners into phosphoinositide-rich membrane subdomains. Although this study primarily focuses on VAMP3 regulation, identification of VAMP7 as another potential R-SNARE-binding partner of PI4K2A raises the possibility that a more general pattern exists whereby interactions between SNARE molecules and lipid kinases contribute to fidelity of membrane fusion. Future studies will be needed to address this possibility.

MATERIALS AND METHODS
Reagents and Antibodies
NEM was purchased from Sigma-Aldrich (St. Louis, MO). Rapamycin was from Calbiochem (Billerica, MA). PIK93 synthesis was performed as previously described (Knight et al., 2006). Rabbit anti-PI4K2A polyclonal antibody was a kind gift from Pietro De Camilli (Yale School of Medicine, New Haven, CT). Mouse anti-HA epitope was purchased from Covance (Princeton, NJ). Alexa-Fluor-488-conjugated goat anti-mouse-IgG and Alexa-Fluor-568-conjugated goat anti-rabbit-IgG secondary antibodies were from Invitrogen/Life Technologies (Carlsbad, CA). PerCP-conjugated goat anti-rabbit-IgG antibody was from Jackson ImmunoResearch (West Grove, PA). Rat monoclonal anti-GFP antibody was from ChromoTek (Martinsried, Germany), whereas rabbit polyclonal antibody against VAMP3 was obtained from the Synaptic Systems (Goettingen, Germany). Mouse anti-Vti1a was from BD Transduction Labs (San Jose, CA) and mouse antibody against PI4K2A was purified from the ATCC hybridoma cell line clone 4C5G (Manassas, VA).

Cell culture and transfection procedures
COS-7 cells were grown on 25-mm glass coverslips and transfected with 0.5 µg of plasmid DNA using the Lipofectamine 2000 reagent

(Invitrogen, Carlsbad, CA) according to the manufacturer's instructions. Knockdown of PI4K2A was performed using PI4K2A siRNA duplexes as described previously (Balla et al., 2005), whereas control siRNA duplexes (AllStars RNAi control) were obtained from Qiagen (Valencia, CA). COS-7 cells were transfected with 20 µl of 20 µM siRNA oligonucleotides using Oligofectamine (Invitrogen, Carlsbad, CA). Knockdown was repeated 1 day later, and live cells were studied by confocal microscopy on the fourth day. PI4K2A expression levels were determined in parallel dishes by western blot analysis.

DNA constructs
The GFP–PI4K2A wild-type and kinase-dead enzyme were as described previously (Balla et al., 2002). The human VAMP3 construct with an HA tag fused to the extracellular C-terminus was generated by subcloning VAMP3 into a pEGFP-N1 backbone vector containing an HA epitope sequence in the place of the GFP sequence between the *Xma*I and *Not*I restriction sites. Human mRFP–FKBP12–Sac1, Tgn38–FRB–CFP, mRFP–FKBP12 and LAMP-1–mRFP have been previously described (Jović et al., 2012; Szentpetery et al., 2010). GFP–VAMP3 and GFP–VAMP3 VW mutant constructs were kindly provided by Heike Folsch (Northwestern University, Chicago, IL). The construct encoding the TeNT light chain was a gift from Thomas Binz (Medizinische Hochschule, Hannover, Germany).

Confocal microscopy analysis and transferrin uptake studies
For live-cell microscopy, COS-7 cells were cultured on 25-mm glass coverslips, and transfected as described above. Cells were washed in modified Krebs-Ringer buffer (120 mM NaCl, 4.7 mM KCl, 1.2 mM CaCl2, 0.7 mM MgSO4, 10 mM glucose, 10 mM Na-Hepes pH 7.4) and cells on coverslips were mounted onto live-cell Attofluor microscopy chambers (Invitrogen, Carlsbad, CA). All live-cell experiments were performed on a heated stage in Krebs-Ringer medium with the controlled temperature, and the objective heater (Bioptech, Butler, PA), kept at

35℃. An inverted Zeiss LSM-510 scanning laser confocal microscope (Carl Zeiss, Thornwood, NY) was used for imaging.

For immunostaining, COS-7 cells were grown on coverslips and fixed in 4% paraformaldehyde (PFA) in PBS, pH 7.4, for 10 min at room temperature. Subsequent staining with primary and secondary antibodies was performed using a staining solution (0.5% BSA with 0.2% saponin).

Transferrin uptake studies were performed in COS-7 cells previously treated for 4 days with PI4K2A or control siRNA duplexes. After a 30-min incubation in serum-free Dulbecco's modified Eagle medium (DMEM), cells were placed in DMEM with 10% fetal bovine serum (FBS) containing Alexa-Fluor-488-conjugated transferrin from human serum for 10 min (immunocytochemistry) or 30 min (flow cytometry), followed by fixation with 4% PFA. Quantification of transferrin levels at the ERC was performed by calculating the ratio of the mean pixel intensity for the ERC pool of transferrin (F_{ERC}) to the mean pixel intensity for the entire cell (F_{total}), using ImageJ software. F_{ERC} was calculated by selecting a region of interest (ROI) encircling an area 2 μm from the nucleus, as determined by DAPI staining. F_{total} for each cell was calculated using an ROI mask for the cell outline, as determined by staining with phalloidin–Rhodamine.

FRAP experiments were performed on an inverted Zeiss LSM-510 confocal microscope, with images collected at 5-s intervals. Photobleaching was performed at 100% intensity of the bleaching laser (488 nm). FRAP traces were calculated from intensity values obtained in the center of a larger bleached area, following the background subtraction. Recovery of fluorescence was calculated as a ratio of fluorescence at time t (F_t) to the initial fluorescence prior to bleaching (F_0) at the ROI.

Flow cytometry

Measurement of VAMP3 surface levels by flow cytometry was performed on COS-7 cells at sub-confluent density previously treated with PI4K2A or control siRNA duplexes, as described above. At 1 day after the second knockdown treatment, cells were transfected with extracellularly tagged VAMP3, VAMP3–HA. The following day cells were trypsinized, pelleted and fixed in 4% PFA prior to staining with mouse anti-HA antibody. Staining was performed either with non-permeabilizing surface staining solution (0.5% BSA) or using permeabilizing solution (0.5% BSA and 0.2% saponin), in both cases followed by staining with rabbit anti-PI4K2A antibody in permeabilized cells. Secondary antibody staining was performed using Alexa-Fluor-488-conjugated goat anti-mouse-IgG secondary antibody together with PerCP-conjugated goat anti-rabbit-IgG antibody. Data acquisition was performed on a Becton Dickinson FACScan cytometer (Franklin Lakes, NJ) using CELLQuest software, processing 10,000 cells per sample.

Immunoprecipitation and western blot analysis

COS-7 cells were co-transfected with the GFP–VAMP3 construct together with either HA–PI4K2A wt or the kinase dead mutant 24 h prior to lysis. Alternatively, COS-7 cells treated for PI4K2A or control knockdown were transfected with GFP–VAMP3 and treated with 1 mM NEM 30 min prior to lysis. Cell lysates were prepared in ice-cold lysis buffer (50 mM Tris-HCl pH 7.4, 150 mM NaCl, 1 mM EDTA, 0.25% deoxycholate, 1% Nonidet P-40, 1 mM Na3VO4, 1 mM dithiothreitol, 10 μg/ml aprotinin, 10 μg/ml leupeptin) and incubated for 1 h with anti-GFP agarose beads (GFP–TRAP; ChromoTek, Martinsried, Germany). Samples were washed five times with cold lysis buffer and bound proteins were then eluted by heating in SDS-PAGE sample buffer at 70℃ for 10 min, resolved by SDS-PAGE and transferred onto nitrocellulose membrane. Rat monoclonal anti-GFP, mouse anti-HA epitope and mouse anti-Vti1a antibodies were used to visualize expressed proteins using the Odyssey infrared detection system.

Affinity purification and mass spectrometric analysis

Transfection, selection of stably transfected FLAG–PI4KA, and FLAG affinity purification were performed as described previously (Goudreault et al., 2009). Samples were analyzed on a Thermo-Finnigan LTQ.

Acquired RAW files were converted to mgf format, which were searched with the Mascot search engine (Matrix Sciences, London, UK) against the human RefSeq database (release 37) with a precursor ion mass tolerance of 3.0 Da, and a fragment ion mass tolerance of 0.6 Da. Methionine oxidation was allowed as a variable modification, and trypsin specificity (with two missed cleavage sites allowed) was selected. The data was analyzed in the 'Analyst' module of ProHits (Liu et al., 2010).

Data were exported into Excel files and manually curated. Biological duplicates of FLAG–PI4K2A were analyzed. To generate lists of high-confidence specific interactors, proteins detected in any of the FLAG-alone samples ($n=8$) were subtracted from the final list. In addition, proteins detected with >10% occurrence in an internal Samuel Lunenfeld Research Institute database of human FLAG interactors that contains >4000 independent AP-MS experiments were removed. Proteins that appeared in both PI4K2A AP-MS runs are shown in Fig. 1 and supplementary material Table S1 ($n=2$). Proteins with a Mascot score of less than 80 were removed. Only those proteins that were detected with at least one unique peptide in both independent biological replicates are reported.

References

Balla, A. and Balla, T. (2006). Phosphatidylinositol 4-kinases: old enzymes with emerging functions. *Trends Cell Biol.* **16**, 351-361.

Balla, A., Tuymetova, G., Barshishat, M., Geiszt, M. and Balla, T. (2002). Characterization of type II phosphatidylinositol 4-kinase isoforms reveals association of the enzymes with endosomal vesicular compartments. *J. Biol. Chem.* **277**, 20041-20050.

Balla, A., Tuymetova, G., Tsiomenko, A., Várnai, P. and Balla, T. (2005). A plasma membrane pool of phosphatidylinositol 4-phosphate is generated by phosphatidylinositol 4-kinase type-III alpha: studies with the PH domains of the oxysterol binding protein and FAPP1. *Mol. Biol. Cell* **16**, 1282-1295.

Balla, A., Kim, Y. J., Varnai, P., Szentpetery, Z., Knight, Z., Shokat, K. M. and Balla, T. (2008). Maintenance of hormone-sensitive phosphoinositide pools in the plasma membrane requires phosphatidylinositol 4-kinase IIIalpha. *Mol. Biol. Cell* **19**, 711-721.

Barylko, B., Gerber, S. H., Binns, D. D., Grichine, N., Khvotchev, M., Südhof, T. C. and Albanesi, J. P. (2001). A novel family of phosphatidylinositol 4-kinases conserved from yeast to humans. *J. Biol. Chem.* **276**, 7705-7708.

Bethani, I., Lang, T., Geumann, U., Sieber, J. J., Jahn, R. and Rizzoli, S. O. (2007). The specificity of SNARE pairing in biological membranes is mediated by both proof-reading and spatial segregation. *EMBO J.* **26**, 3981-3992.

Brandhorst, D., Zwilling, D., Rizzoli, S. O., Lippert, U., Lang, T. and Jahn, R. (2006). Homotypic fusion of early endosomes: SNAREs do not determine fusion specificity. *Proc. Natl. Acad. Sci. USA* **103**, 2701-2706.

Burgess, J., Del Bel, L. M., Ma, C. I., Barylko, B., Polevoy, G., Rollins, J., Albanesi, J. P., Krämer, H. and Brill, J. A. (2012). Type II phosphatidylinositol 4-kinase regulates trafficking of secretory granule proteins in Drosophila. *Development* **139**, 3040-3050.

Craige, B., Salazar, G. and Faundez, V. (2008). Phosphatidylinositol-4-kinase type II alpha contains an AP-3-sorting motif and a kinase domain that are both required for endosome traffic. *Mol. Biol. Cell* **19**, 1415-1426.

Ellena, J. F., Liang, B., Wiktor, M., Stein, A., Cafiso, D. S., Jahn, R. and Tamm, L. K. (2009). Dynamic structure of lipid-bound synaptobrevin suggests a nucleation-propagation mechanism for trans-SNARE complex formation. *Proc. Natl. Acad. Sci. USA* **106**, 20306-20311.

Fasshauer, D., Sutton, R. B., Brunger, A. T. and Jahn, R. (1998). Conserved structural features of the synaptic fusion complex: SNARE proteins reclassified as Q- and R-SNAREs. *Proc. Natl. Acad. Sci. USA* **95**, 15781-15786.

Fasshauer, D., Antonin, W., Margittai, M., Pabst, S. and Jahn, R. (1999). Mixed and non-cognate SNARE complexes. Characterization of assembly and biophysical properties. *J. Biol. Chem.* **274**, 15440-15446.

Feng, D., Crane, K., Rozenvayn, N., Dvorak, A. M. and Flaumenhaft, R. (2002). Subcellular distribution of 3 functional platelet SNARE proteins: human cellubrevin, SNAP-23, and syntaxin 2. *Blood* **99**, 4006-4014.

Galli, T., Chilcote, T., Mundigl, O., Binz, T., Niemann, H. and De Camilli, P. (1994). Tetanus toxin-mediated cleavage of cellubrevin impairs exocytosis of transferrin receptor-containing vesicles in CHO cells. *J. Cell Biol.* **125**, 1015-1024.

Ganley, I. G., Espinosa, E. and Pfeffer, S. R. (2008). A syntaxin 10-SNARE complex distinguishes two distinct transport routes from endosomes to the trans-Golgi in human cells. *J. Cell Biol.* **180**, 159-172.

Gillooly, D. J., Morrow, I. C., Lindsay, M., Gould, R., Bryant, N. J., Gaullier, J. M., Parton, R. G. and Stenmark, H. (2000). Localization of phosphatidylinositol 3-phosphate in yeast and mammalian cells. *EMBO J.* **19**, 4577-4588.

Gillooly, D. J., Raiborg, C. and Stenmark, H. (2003). Phosphatidylinositol 3-phosphate is found in microdomains of early endosomes. *Histochem. Cell Biol.* **120**, 445-453.

Gordon, D. E., Mirza, M., Sahlender, D. A., Jakovleska, J. and Peden, A. A. (2009). Coiled-coil interactions are required for post-Golgi R-SNARE trafficking. *EMBO Rep.* **10**, 851-856.

Goudreault, M., D'Ambrosio, L. M., Kean, M. J., Mullin, M. J., Larsen, B. G., Sanchez, A., Chaudhry, S., Chen, G. I., Sicheri, F., Nesvizhskii, A. I. et al. (2009). A PP2A phosphatase high density interaction network identifies a novel striatin-interacting phosphatase and kinase complex linked to the cerebral cavernous malformation 3 (CCM3) protein. *Mol. Cell. Proteomics* **8**, 157-171.

Guo, J., Wenk, M. R., Pellegrini, L., Onofri, F., Benfenati, F. and De Camilli, P. (2003). Phosphatidylinositol 4-kinase type IIalpha is responsible for the phosphatidylinositol 4-kinase activity associated with synaptic vesicles. *Proc. Natl. Acad. Sci. USA* **100**, 3995-4000.

Hsu, V. W., Bai, M. and Li, J. (2012). Getting active: protein sorting in endocytic recycling. *Nat. Rev. Mol. Cell Biol.* **13**, 323-328.

Inoue, T., Heo, W. D., Grimley, J. S., Wandless, T. J. and Meyer, T. (2005). An inducible translocation strategy to rapidly activate and inhibit small GTPase signaling pathways. *Nat. Methods* **2**, 415-418.

Jović, M., Kean, M. J., Szentpetery, Z., Polevoy, G., Gingras, A. C., Brill, J. A. and Balla, T. (2012). Two phosphatidylinositol 4-kinases control lysosomal delivery of the Gaucher disease enzyme, β-glucocerebrosidase. *Mol. Biol. Cell* **23**, 1533-1545.

Knight, Z. A., Gonzalez, B., Feldman, M. E., Zunder, E. R., Goldenberg, D. D., Williams, O., Loewith, R., Stokoe, D., Balla, A., Toth, B. et al. (2006). A pharmacological map of the PI3-K family defines a role for p110alpha in insulin signaling. *Cell* **125**, 733-747.

Komatsu, T., Kukelyansky, I., McCaffery, J. M., Ueno, T., Varela, L. C. and Inoue, T. (2010). Organelle-specific, rapid induction of molecular activities and membrane tethering. *Nat. Methods* **7**, 206-208.

Liu, G., Zhang, J., Larsen, B., Stark, C., Breitkreutz, A., Lin, Z. Y., Breitkreutz, B. J., Ding, Y., Colwill, K., Pasculescu, A. et al. (2010). ProHits: integrated software for mass spectrometry-based interaction proteomics. *Nat. Biotechnol.* **28**, 1015-1017.

Mallard, F., Tang, B. L., Galli, T., Tenza, D., Saint-Pol, A., Yue, X., Antony, C., Hong, W., Goud, B. and Johannes, L. (2002). Early/recycling endosomes-to-TGN transport involves two SNARE complexes and a Rab6 isoform. *J. Cell Biol.* **156**, 653-664.

Martinez-Arca, S., Rudge, R., Vacca, M., Raposo, G., Camonis, J., Proux-Gillardeaux, V., Daviet, L., Formstecher, E., Hamburger, A., Filippini, F. et al. (2003). A dual mechanism controlling the localization and function of exocytic v-SNAREs. *Proc. Natl. Acad. Sci. USA* **100**, 9011-9016.

Maxfield, F. R. and McGraw, T. E. (2004). Endocytic recycling. *Nat. Rev. Mol. Cell Biol.* **5**, 121-132.

Mayer, A., Wickner, W. and Haas, A. (1996). Sec18p (NSF)-driven release of Sec17p (alpha-SNAP) can precede docking and fusion of yeast vacuoles. *Cell* **85**, 83-94.

McMahon, H. T., Ushkaryov, Y. A., Edelmann, L., Link, E., Binz, T., Niemann, H., Jahn, R. and Südhof, T. C. (1993). Cellubrevin is a ubiquitous tetanus-toxin substrate homologous to a putative synaptic vesicle fusion protein. *Nature* **364**, 346-349.

McNew, J. A., Parlati, F., Fukuda, R., Johnston, R. J., Paz, K., Paumet, F., Söllner, T. H. and Rothman, J. E. (2000). Compartmental specificity of cellular membrane fusion encoded in SNARE proteins. *Nature* **407**, 153-159.

Miller, S. E., Sahlender, D. A., Graham, S. C., Höning, S., Robinson, M. S., Peden, A. A. and Owen, D. J. (2011). The molecular basis for the endocytosis of small R-SNAREs by the clathrin adaptor CALM. *Cell* **147**, 1118-1131.

Minogue, S., Waugh, M. G., De Matteis, M. A., Stephens, D. J., Berditchevski, F. and Hsuan, J. J. (2006). Phosphatidylinositol 4-kinase is required for endosomal trafficking and degradation of the EGF receptor. *J. Cell Sci.* **119**, 571-581.

Naughtin, M. J., Sheffield, D. A., Rahman, P., Hughes, W. E., Gurung, R., Stow, J. L., Nandurkar, H. H., Dyson, J. M. and Mitchell, C. A. (2010). The myotubularin phosphatase MTMR4 regulates sorting from early endosomes. *J. Cell Sci.* **123**, 3071-3083.

Pan, W., Choi, S. C., Wang, H., Qin, Y., Volpicelli-Daley, L., Swan, L., Lucast, L., Khoo, C., Zhang, X., Li, L. et al. (2008). Wnt3a-mediated formation of phosphatidylinositol 4,5-bisphosphate regulates LRP6 phosphorylation. *Science* **321**, 1350-1353.

Parlati, F., Varlamov, O., Paz, K., McNew, J. A., Hurtado, D., Söllner, T. H. and Rothman, J. E. (2002). Distinct SNARE complexes mediating membrane fusion in Golgi transport based on combinatorial specificity. *Proc. Natl. Acad. Sci. USA* **99**, 5424-5429.

Poirier, M. A., Xiao, W., Macosko, J. C., Chan, C., Shin, Y. K. and Bennett, M. K. (1998). The synaptic SNARE complex is a parallel four-stranded helical bundle. *Nat. Struct. Biol.* **5**, 765-769.

Polgár, J., Chung, S. H. and Reed, G. L. (2002). Vesicle-associated membrane protein 3 (VAMP-3) and VAMP-8 are present in human platelets and are required for granule secretion. *Blood* **100**, 1081-1083.

Regazzi, R., Sadoul, K., Meda, P., Kelly, R. B., Halban, P. A. and Wollheim, C. B. (1996). Mutational analysis of VAMP domains implicated in Ca2+-induced insulin exocytosis. *EMBO J.* **15**, 6951-6959.

Rothenberger, F., Velic, A., Stehberger, P. A., Kovacikova, J. and Wagner, C. A. (2007). Angiotensin II stimulates vacuolar H+ -ATPase activity in renal acid-secretory intercalated cells from the outer medullary collecting duct. *J. Am. Soc. Nephrol.* **18**, 2085-2093.

Ryder, P. V., Vistein, R., Gokhale, A., Seaman, M. N., Puthenveedu, M. A. and Faundez, V. (2013). The WASH complex, an endosomal Arp2/3 activator, interacts with the Hermansky-Pudlak syndrome complex BLOC-1 and its cargo phosphatidylinositol-4-kinase type IIα. *Mol. Biol. Cell* **24**, 2269-2284.

Salazar, G., Zlatic, S., Craige, B., Peden, A. A., Pohl, J. and Faundez, V. (2009). Hermansky-Pudlak syndrome protein complexes associate with phosphatidylinositol 4-kinase type II alpha in neuronal and non-neuronal cells. *J. Biol. Chem.* **284**, 1790-1802.

Simons, J. P., Al-Shawi, R., Minogue, S., Waugh, M. G., Wiedemann, C., Evangelou, S., Loesch, A., Sihra, T. S., King, R., Warner, T. T. et al. (2009). Loss of phosphatidylinositol 4-kinase 2alpha activity causes late onset degeneration of spinal cord axons. *Proc. Natl. Acad. Sci. USA* **106**, 11535-11539.

Söllner, T., Bennett, M. K., Whiteheart, S. W., Scheller, R. H. and Rothman, J. E. (1993). A protein assembly-disassembly pathway in vitro that may correspond to sequential steps of synaptic vesicle docking, activation, and fusion. *Cell* **75**, 409-418.

Sutton, R. B., Fasshauer, D., Jahn, R. and Brunger, A. T. (1998). Crystal structure of a SNARE complex involved in synaptic exocytosis at 2.4 A resolution. *Nature* **395**, 347-353.

Szentpetery, Z., Várnai, P. and Balla, T. (2010). Acute manipulation of Golgi phosphoinositides to assess their importance in cellular trafficking and signaling. *Proc. Natl. Acad. Sci. USA* **107**, 8225-8230.

Vicogne, J., Vollenweider, D., Smith, J. R., Huang, P., Frohman, M. A. and Pessin, J. E. (2006). Asymmetric phospholipid distribution drives in vitro reconstituted SNARE-dependent membrane fusion. *Proc. Natl. Acad. Sci. USA* **103**, 14761-14766.

Volchuk, A., Sargeant, R., Sumitani, S., Liu, Z., He, L. and Klip, A. (1995). Cellubrevin is a resident protein of insulin-sensitive GLUT4 glucose transporter vesicles in 3T3-L1 adipocytes. *J. Biol. Chem.* **270**, 8233-8240.

Wang, Y. J., Wang, J., Sun, H. Q., Martinez, M., Sun, Y. X., Macia, E., Kirchhausen, T., Albanesi, J. P., Roth, M. G. and Yin, H. L. (2003). Phosphatidylinositol 4 phosphate regulates targeting of clathrin adaptor AP-1 complexes to the Golgi. *Cell* **114**, 299-310.

Xu, H. and Wickner, W. (2010). Phosphoinositides function asymmetrically for membrane fusion, promoting tethering and 3Q-SNARE subcomplex assembly. *J. Biol. Chem.* **285**, 39359-39365.